INSTITUTE OF PHYSICS PUBLISHING JOURNAL OF PHYSICS D: APPLIED PHYSICS

J. Phys. D: Appl. Phys. **37** (2004) 3233–3243 PII: S0022-3727(04)82731-1

Liquid-jet laser–plasma extreme ultraviolet sources: from droplets to filaments

Björn A M Hansson[1] **and Hans M Hertz**

Biomedical and X-Ray Physics, Royal Institute of Technology/Albanova, S-10691 Stockholm, Sweden

E-mail: hertz@biox.kth.se and bhansson@cymer.com

Received 28 June 2004, in final form 29 September 2004
Published 19 November 2004
Online at stacks.iop.org/JPhysD/37/3233
doi:10.1088/0022-3727/37/23/004

Abstract
The laser plasma is one of the major contenders as a high-power source for future high-volume-manufacturing extreme ultraviolet lithography systems. Such laser–plasma sources require a target system that allows high-repetition-rate operation with low debris and manageable thermal load at the required high laser power. In this paper, we review the development of the liquid-jet target laser plasmas, from droplets to filaments, with special emphasis on its applicability for high-power extreme ultraviolet generation. We focus on two target systems, the liquid-xenon-jet and the liquid-tin-jet.

1. Introduction

At present, extreme ultraviolet lithography (EUVL) is considered a strong contender for high-volume semiconductor manufacturing at the 32 nm node around 2010 (see, e.g. [1]). However, the availability of high-power sources remains one of the main areas of concern that must be solved for this technology to be successful. In many respects, the requirements on the source for EUVL exposure tools are much more demanding than for other short-wavelength applications, such as, e.g. soft x-ray microscopy, x-ray photoemission spectroscopy or low-power extreme ultraviolet (EUV) metrology applications. Key issues for high-volume EUVL sources include the generation of sufficient power and the reduction of damaging debris.

In this paper, we review the development and current status of EUV laser–plasma sources based on liquid-jet targets, with special emphasis on their applicability in high-volume EUVL tools. With liquid-jet targets we refer to all targets achieved by ejecting a collimated liquid jet through a nozzle although the jet may further break up into a train of droplets or freeze to a solid filament. The paper focuses on the authors' extensive work on liquid-xenon-jet laser–plasma sources and the more limited work on liquid-tin-jet laser plasmas.

[1] Present address: Cymer Inc., 17075 Thornmint Ct., San Diego, CA 92127, USA.

Liquid-jet laser–plasma sources have a number of generic advantages that are of importance for EUVL. It is a regenerative target that allows high-repetition-rate laser–plasma operation over extended periods of time. Many different target materials can be used, thereby allowing spectral tailoring of the emitted radiation. For high-power EUVL applications this source type has a few additional key strengths. First, the liquid-jet technology allows the transportation of target material in a collimated fashion to a plasma interaction point at a significant distance from other hardware. This is especially important in order to handle the high thermal load from the plasma and to allow for non-obscured collection of the generated radiation. Furthermore, only a limited amount of target material is used due to the microscopic nature of the target. This limits the production of harmful debris. Finally, the collimated target transport allows for the generation of a small plasma that is also a prerequisite for high collection angles.

2. Laser–plasma systems for EUV generation

In a laser plasma, the plasma is created through the interaction of short high-peak-power laser pulses with a target. Pulse energies of the order of 1 J with pulse lengths of several nanoseconds are typically used, leading to peak powers in the 100 MW regime. Furthermore, by focusing the laser pulses down to diameters in the 100 μm range, power densities

of 10^{11}–10^{12} W cm^{-2} are achieved. These power densities are sufficient to raise the temperature of the plasmas to several 100 000 K suitable for emission in the EUV wavelength region [2]. The target can basically be any substance in any state as long as the density is high enough to reach a sufficient plasma density. However, the choice of target material will influence both the emission spectrum of the plasma as well as the contamination impact on optical components in the vicinity of the plasma. These aspects will be discussed in more detail further on in this paper.

For a laser–plasma source intended as a light source in a high-volume-manufacturing EUVL stepper, the form in which the target material is delivered is important. The reason for this is that new target material has to be available for each new laser shot, and a stepper is estimated to operate at a multi-kilohertz repetition rate, with 25% duty cycle basically 24 h a day [3]. Traditionally, when only single-shot experiments were sufficient for basic research purposes, solid bulk targets were employed. These targets are typically translated between each shot to provide a fresh target surface and can, therefore, only operate for a very limited time until the whole surface is filled with craters. In addition, particulate debris, i.e. large fractions of solid or molten material may be ejected from the plasma region due to the induced shock wave reflected in the bulk material [4].

An alternative to the bulk targets is to use a thin tape as a target, as illustrated in figure 1(*a*), where a new tape surface can be continuously supplied, at least until the tape runs out. The tape target further limits the debris by allowing the shock wave created by the plasma to escape through the tape rather than be reflected back to the surface [4]. However, the debris emission from a tape target is still substantial [5]. In addition, tape targets are limited to materials that can be processed into a tape and in operation time.

Thus, a target delivery system is needed that continuously supplies new target material to the point of plasma formation, and reduces debris. This leads us to target systems based on gases and liquids.

For gaseous target materials, the gas-puff target is an alternative as illustrated in figure 1(*b*) [6]. The clear advantage is that no larger debris particles can be ejected from the plasma target. However, the laser has to be focused close to the nozzle in order for the target gas to have sufficient density for effective laser–plasma generation. This may lead to sputtering of nozzle material that, in turn, may coat sensitive components [7]. Under the right operating conditions, the gas will form clusters enhancing the EUV production from the gas target [8–10].

A similar target is the liquid-spray target (cf figure 1(*c*)), which can be applied to liquids or condensed gases, where larger droplets are formed. Compared to the gas/cluster target, this target has the advantage of higher target density, leading to improved EUV generation, and better collimation of the target flow allowing for slightly longer working distances, although still in the range of a few millimetres [11, 12].

This paper, however, describes laser plasmas based on liquid-jet targets, both in the form of droplets, as in figure 1(*d*), and jets/filaments, as in figure 1(*e*). Such regenerative high-density target systems allow high-repetition-rate operation for extended periods of time and reduce debris by using microscopic target dimensions [13, 14]. For EUV lithography applications a major advantage is that target material is transported in a collimated fashion to the point in space where it interacts with the laser pulse. In this way, the plasma operation can take place at large distances from any source hardware. This will limit both the thermal load from the plasma on to any other source component as well as ion sputtering.

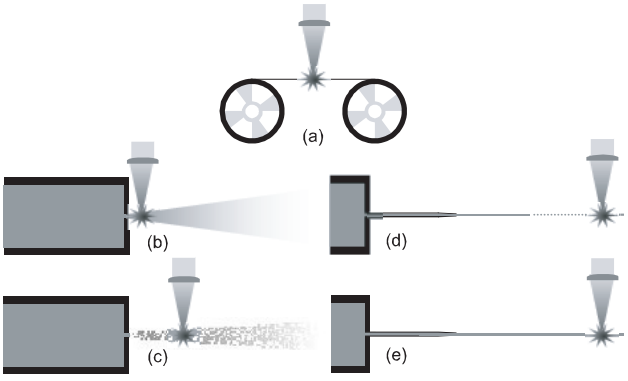

Figure 1. Different target geometries for laser–plasma generation: (*a*) tape target, (*b*) gas/cluster target, (*c*) liquid-spray target, (*d*) liquid-jet target and (*e*) liquid-droplet target.

3. Liquid-jet targets

A liquid jet is formed by urging a liquid through a small nozzle orifice by applying a certain drive pressure, thereby creating a jet. Such jets and their breakup behaviour have been described in several papers, e.g. [15]. At high speeds different mechanisms lead to unstable jet oscillations or sprays [16]. In the following we focus on lower speed jets. Here, the collimated jet spontaneously breaks up into uniformly spaced drops due to the minimization of surface energy (Rayleigh-type breakup) [17], as illustrated in figure 2. The general theory for the droplet formation distance, L, is that of Weber [18, 19] as discussed in [20]:

$$L > 3.5v\left[\left(\frac{\rho d^3}{\sigma}\right)^{0.5} + \left(\frac{3\eta d}{\sigma}\right)\right], \tag{1}$$

where v is the jet velocity, ρ the density of the liquid, d the jet diameter, σ the surface tension of the liquid and η is the viscosity of the liquid. Furthermore, the droplets tend to be generated at a spontaneous drop-formation frequency, f, given by [17]

$$f = \frac{v}{\lambda} = \frac{v}{4.51 \times d}, \tag{2}$$

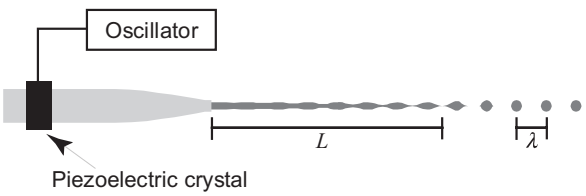

Figure 2. Rayleigh-type breakup of a liquid jet where the drop-formation frequency is stimulated with a piezoelectric crystal.

where λ is the distance between the droplets. However, the spontaneous drop-formation frequency is not sufficiently stable to allow for precise targeting of the droplets. The droplet formation is, therefore, typically stimulated by an added periodical disturbance of the jet to control the drop frequency. This can, for example, be achieved with a piezoelectric crystal as shown in figure 2. By applying a large disturbance it is also possible to generate droplets with a frequency significantly different from the spontaneous frequency. Droplets were first used as a laser–plasma target for short-wavelength-generation in the water window utilizing carbon and nitrogen ion emission from ethanol and ammonia, respectively [13, 21] and in the EUV employing oxygen ion emission from water/methanol mixtures [22] and, later, from water [23].

A key advantage with the liquid-droplet target is that it is an example of a mass-limited target [24] if the droplets are small enough to contain the minimum number of atoms required for efficient EUV generation. In that case, the droplet is completely ionized and no particulate debris is generated. The liquid-droplet target was, quite early on, shown to limit the debris deposition compared to a tape target by a factor of 200–300 [25]. Actually, droplet targets for laser–plasma interaction had already been demonstrated in the 1970s [26–28], however, not with the aim to generate soft x-ray and EUV radiation but rather for nuclear fusion.

Instead of targeting individual droplets, the jet itself can be targeted if the laser is focused before the droplet formation point [14,29] (cf figure 1(*e*)). An advantage of this approach is that the laser pulses do not have to be temporally synchronized with the droplet frequency. Furthermore, liquids with low surface tension or unstable droplet formation may be used. The disadvantage is, however, that for many liquids with common surface tension and thus millimetre-length drop-formation distances, the laser has to be focused close to the nozzle, which may induce thermal or sputtering problems. An exception is when cryogenic substances such as, for example, xenon are used since the jet may freeze to a solid filament before the drop formation point due to evaporative cooling. Liquid nitrogen [30], liquid xenon [31,32], and liquid argon [33] were the first cryogenic liquids employed for liquid-jet laser–plasma operation.

The evaporative cooling and freezing of the jet may be modelled using elementary thermodynamic arguments. Assuming xenon with an initial temperature of 170 K and an injection pressure of 30 bar, the calculated cooling/freezing process as a function of distance from the nozzle orifice is illustrated in figure 3. Details of the model are described by Hansson *et al* [20]. In addition, the minimum droplet-formation distance according to equation (2) is shown in figure 3. As can be seen, the jet will rapidly freeze, thereby inhibiting droplet formation. The jet velocity is calculated from the injection pressure according to [34].

Although the cooling/freezing calculations contain some uncertainties (cf [20]), it is still clear that the model predicts that the jet freezes well before the droplet formation point. This is supported by experimental evidence shown in figure 4. Here the xenon jet is photographed several centimetres from the nozzle orifice. The image is taken through a microscope, using a ∼10 ns laser pulse for illumination. At this distance, the jet is broken at several locations but no sign of general droplet formation is visible. This behaviour is only possible if the jet is in the solid state.

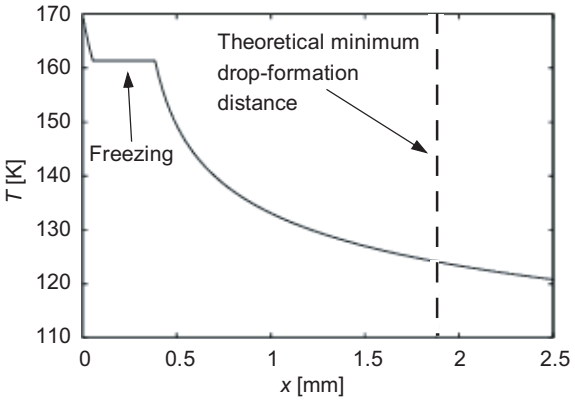

Figure 3. The calculated cooling process of a 10 μm xenon jet injected into vacuum at 30 bar corresponding to 40 m s^{-1}. The theoretical model indicates that the jet freezes well before the droplet formation point, thereby inhibiting the formation of droplets (from [20]).

Figure 4. A 10 ns flash photograph of a xenon jet several centimetres from the nozzle orifice. The jet is broken at several locations but no signs of general droplet formation are visible (from [20]).

Droplets of liquefied gases, such as xenon, can be generated if the jet is injected into an environment where the pressure is closer to the vapour pressure of the liquid at the temperature of the jet, and therefore the effective evaporation rate is lower. This was first shown for oxygen and argon [26]. However, the required ambient pressure is much too high for laser–plasma soft-x-ray and EUV generation purposes since the emitted radiation will rapidly be absorbed in the surrounding gas. Droplets may be produced in a high-vacuum environment using a differential pumping scheme, where the drops are formed in a chamber with higher pressure and then injected into high vacuum [26, 35]. However, with such a scheme it may be difficult to achieve acceptable spatial stability so that the drops can be accurately targeted by the laser pulses since it has been reported that the drop flight path is perturbed during injection [36] into high vacuum. This is somewhat supported in [37], which shows conversion efficiency (CE) measurements of xenon droplets but concludes that stability will be a major challenge for such a source. However, recent studies by Endo [38] and Stamm [39] illustrating xenon-droplet targets may indicate that Xe droplets are being re-evaluated, although no stability data are given in these reports.

Finally, we note that liquid jets can be operated in a collimated fashion with surprisingly high jet speeds when operated in a vacuum environment [16]. This is due to the fact that so-called wind-induced breakup mechanisms are significantly reduced compared to operation in an atmospheric environment. Such very high-speed jets may be important for high-repetition-rate operation (cf section 9).

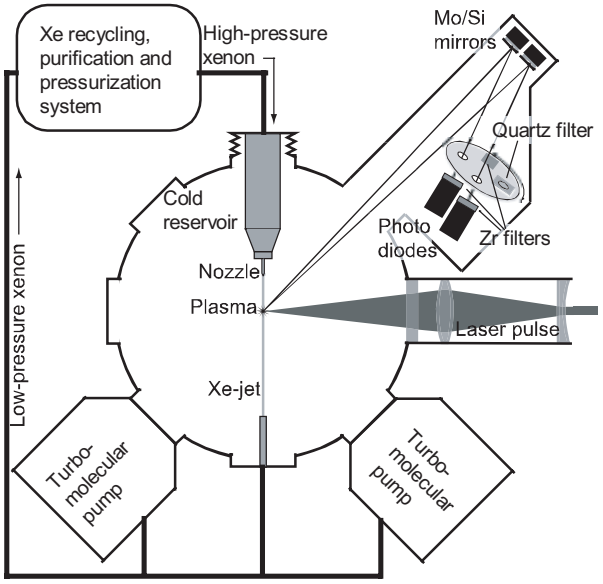

Figure 5. A typical experimental arrangement for liquid-xenon-jet laser–plasma generation and EUV in-band-emission monitoring (from [38]).

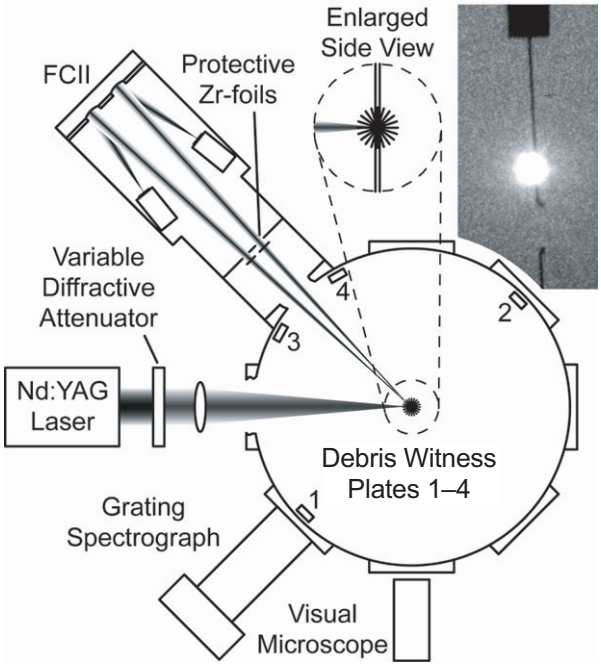

Figure 6. Experimental arrangement of the liquid-metal-jet laser–plasma experiment. The photo shows a double-exposure of the jet and the plasma (from [42]).

4. Experimental arrangements

As mentioned in the introduction, the present article focuses mainly on the extensive work performed by the authors on liquid-xenon-jet laser plasma and the more limited work on liquid-tin-jet laser plasmas. This section, therefore, introduces the typical experimental arrangements for these target systems. In addition, we briefly discuss other target systems.

4.1. Liquid-xenon-jet arrangement

Figure 5 shows a typical experimental arrangement for liquid-xenon-jet laser–plasma generation as reported in [40]. The liquid jet is formed by forcing xenon gas under high pressure into a reservoir cooled to liquefy the xenon. A tapered glass capillary nozzle, with an orifice diameter of typically 10–30 μm, is attached to the reservoir, producing a microscopic liquid jet into an ultra-high vacuum (UHV) compatible chamber. Vacuum is maintained by two $\sim$2000 litre s^{-1} turbomolecular pumps resulting in pressures of 10^{-4}–10^{-3} mbar during operation. The base pressure of the system, before jet operation, is typically in the 10^{-8}–10^{-7} mbar range but could be further reduced, e.g. through baking. To reduce the load on the turbomolecular pumps during operation, the non-evaporated part of the xenon jet is extracted from the chamber through a differential-pumping scheme. The xenon evacuated through both the turbomolecular pumps and the jet-extraction system is further collected by a recycling, purification and pressurization system allowing for closed-loop usage of xenon. Without such a recycling system, the high cost of xenon may limit the experimental time. The plasma is typically generated by focusing Nd : YAG laser pulses with $\lambda = 1064$ nm, $\sim$5 ns pulse length and up to 350 mJ pulse energy onto the jet through a focusing system theoretically capable of obtaining a full-width at half-maximum (FWHM) 10 μm spot. Finally, the EUV emission is generally monitored using a flying circus (FC) tool [41].

Generation of liquid-xenon-jet laser plasmas has also been reported by other authors [37, 39, 42, 43] with correspondingly more or less detailed descriptions of the experimental arrangements.

4.2. Liquid-tin-jet arrangement

Figure 6 shows the experimental arrangement for a liquid-tin-jet laser plasma reported by Jansson *et al* [44]. The liquid-tin-jet is generated by a liquid-metal-jet system consisting of a 0.15 litre high-pressure tank, a sintered stainless-steel particle filter and a 75 μm diameter ruby pin-hole nozzle [45]. The high-pressure tank is enclosed in an IR-radiation heater, capable of heating the tin (99.8%) to up to $>$300°C. The liquid jet is injected into a vacuum chamber, which is evacuated to 10^{-5} mbar by a 500 litre s^{-1} turbo-drag pump, by applying up to 200 bar of nitrogen driving pressure resulting in jet speeds of up to $\sim$75 m s^{-1}. The target is operated in the liquid-jet mode. However, with the addition of a periodic stimulation of the nozzle it could also be operated in the droplet mode.

The plasma is generated by a 20 Hz Nd : YAG laser capable of delivering 300 mJ, $\sim$5 ns pulses at $\lambda = 1064$ nm. The beam is focused onto the liquid-metal jet to a minimum simulated FWHM of $\sim$17 μm. Absolute measurements of the EUV flux are performed using the same FC tool as for xenon [41]. In this case, however, the calibrated equipment inside the UHV compatible FC tool is shielded from the main chamber by an assembly with two Zr-filtered apertures to avoid contamination. By decreasing the radius of one aperture at a time and observing that the relative signal intensities of the FCII diodes do not change, errors due to spatial mismatch are avoided. During the tin experiments one of the apertures is fully closed except for short exposures during data collection, minimizing filter degradation and at the same time

Table 1. The September 2003 EUVL source requirements as jointly agreed by ASML, Canon and Nikon (from [49]).

Source characteristic	Requirement
Wavelength	13.5 nm
EUV power (in-band)	115 W[a]
Repetition frequency	7–10 kHz[c]
Integrated energy stability	$\pm 0.3\%$, 3σ over 50 pulses[b]
Source cleanliness	$\geqslant$30 000 h[b]
Étendue of source output	max 1–3.3 mm^2 sr[c]
Maximum solid angle input to illuminator	0.03–0.2 sr[c]
Spectral purity	
130–400 nm (DUV/UV)	$\leqslant 7\%$[c]
$\geqslant$ 400 nm (IRVis) at wafer	TBD[c]

[a] At IF.
[b] After IF.
[c] Design dependent.

enabling monitoring of potential filter transmission loss of the continuously open aperture.

The authors are not aware of any other laser–plasma results on pure liquid-tin-jets. However, another concept of tin laser–plasma based on tin doped droplets has been presented by Koay *et al* [46]. The article does not specify the actual nature of the droplets, but the published spectra correspond to the spectrum of a $SnCl:H_2O$ solution published in a patent application [47]. Using solutions is an effective way of obtaining liquid-jet targets of different substances [21, 44, 48].

5. Demands on a source for EUV lithography

An EUV source has to meet very demanding requirements to be suitable for operation in production-scale EUVL steppers. An estimation of the final requirements on an EUVL-stepper source is given in table 1, a list of requirements jointly published by the three major stepper manufacturers: ASML, Canon and Nikon [49].

Although all requirements finally have to be fulfilled, the high power required at the intermediate focus (IF) and the source cleanliness are probably the key parameters and the most demanding requirements.

The usable EUV power that will be delivered to the IF is given by

$$P_{\mathrm{IF}} = P_{\mathrm{L}} \times \mathrm{CE} \times \frac{\Omega}{2\pi} \times \left(\frac{A_{\mathrm{col}}}{A_{\mathrm{tot}}}\right) \times R \times T_{\mathrm{SPF}} \times T_{\mathrm{gas}}, \quad (3)$$

where the different parameters will be discussed in more detail below. In brief, the parameters are the drive-laser power, P_{L}, the CE from laser power to in-band usable EUV radiation, CE, the solid angle of the collector as also illustrated in figure 7, Ω, the fraction of collectable source area to the total source area ($A_{\mathrm{col}}/A_{\mathrm{tot}}$), the average reflectivity of the collector, R, the transmission of a spectral-purity filter that may be needed, T_{SPF}, and the transmission of the background gas present in the vacuum chamber, T_{gas}. The parameters are further explained in table 2, which contains a design example of how a laser–plasma source could achieve the required power to the IF. The values selected are typically achievable values for a laser–plasma source and the design example is mainly included to illustrate the high laser powers that generally will be needed to achieve

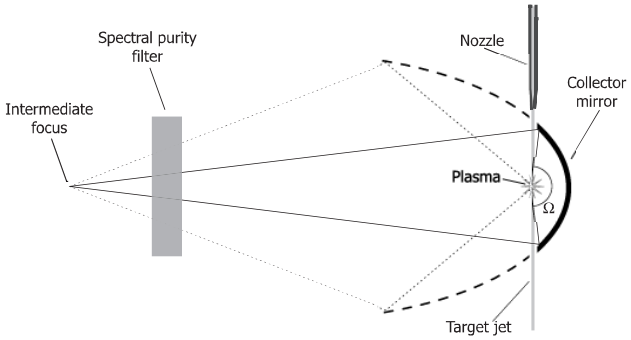

Figure 7. Illustration of how a collector with a large solid angle, Ω, can be used with a liquid-jet laser–plasma source since no source hardware is obscuring the collection angle. The dashed line further illustrates how an additional grazing-incidence collector could theoretically be added to increase the collection angle. Finally, the arrangement also includes a conceptual spectral-purity filter that may filter our non-EUV radiation.

Table 2. Design example of how a laser–plasma source could meet the specified power requirement at the IF.

Laser power, P_{L}	20 kW
Conversion efficiency, CE	2%/(2%BW 2π sr)
Power into 2π sr	400
Collector solid angle, Ω	4 sr
Collectable source-area fraction ($A_{\mathrm{col}}/A_{\mathrm{tot}}$)	100%
Average collector reflectivity, R	50%
Spectral-purity-filter transmission, T_{SPF}	100% (no filter)
Background gas transmission, T_{gas}	90%
Power into IF, P_{IF}	115 W

the requirements. Furthermore, when actual experimental values for the parameters are discussed further on in this paper, they will be related to the values of this design example.

Although achieving the required power is an obvious key requirement, the source cleanliness is of equal importance. In the common source requirement, the source cleanliness is defined after the IF, i.e. for optical components beyond the first collector. However, from a source point of view, the collector lifetime may be the most demanding problem since the collector itself will be facing the plasma directly. Especially if the collector has to be replaced frequently due to contamination from the source, this will increase the cost-of-ownership (CoO) of the source significantly [50]. Damage issues are discussed further in section 8.

6. Conversion efficiency and target material

As is evident from equation (3) the required laser power is inversely proportional to the CE. It is therefore important to achieve the highest possible CE. One major factor determining the CE is the choice of target material since the spectral emission profiles of different materials are quite different.

A general emission feature of atoms of different weight is that lighter elements typically generate narrow-band line radiation and heavier elements a broader quasi-continuum. This is due to the difference in the number of atomic transitions available and the fact that the bremsstrahlung contribution increases with higher atom numbers. The narrow-band emission lines from light elements are well illustrated

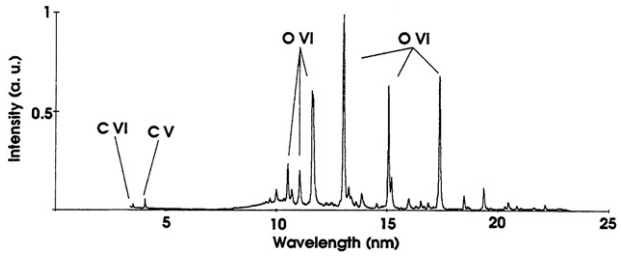

Figure 8. Emission spectrum from water/methanol droplets (from [22]).

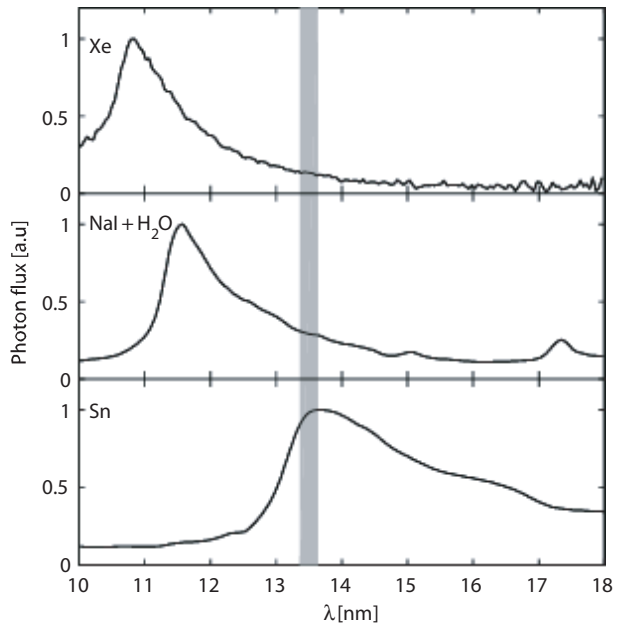

Figure 9. EUV emission spectra from xenon, iodine and tin liquid-jet laser plasmas. The shaded area depicts the 2% bandwidth region around $\lambda = 13.5$ nm with high reflectivity of a Mo/Si multilayer system.

by the emission spectra in figure 8 of $_8$O and $_6$C from a water/methanol droplet laser plasma [22]. The strong OVI emission line at $\lambda = 13$ nm could potentially be very suitable for EUVL since it is significantly narrower than the bandwidth of Mo/Si mirrors. However, unfortunately a CE of only about 0.1% into that emission line and 4π sr has been shown [51–53]. By comparing with the design example of table 2, it is evident that drive-lasers in the hundreds of kilowatt range would be needed with such low CE numbers, which is not feasible.

The quasi-continuum broadband emission from heavier elements is well illustrated in figure 9 with $_{50}$Sn from a liquid-tin-jet target [44], $_{53}$I from a liquid-jet target of sodium iodine dissolved in water [44] and $_{54}$Xe from a liquid-xenon-jet target [54] where the spectra show similar emission profiles for all materials although the peaks are located at shorter wavelengths for the heavier substances. Such profiles have been observed and explained in laser–plasmas from elements ranging from $_{50}$Sn to $_{82}$Pb [55–58].

As is evident from figure 9, xenon is not an optimal target for CE since the emission peak is well below the desired reflectivity bandwidth centred around $\lambda = 13.5$ nm for an EUVL system based on Mo/Si mirrors. The peak is even below the silicon absorption edge near $\lambda = 12.4$ nm making it generally impossible to match Mo/Si mirrors to the peak. However, since xenon is a noble gas, its contamination characteristics still make it interesting as a target material, as is discussed in section 8. Although the spectrum of xenon is not optimal for EUVL, a CE of 0.95%/(2%BW 2π sr) at $\lambda = 13.45$ nm has been reported in [40] with the liquid-xenon-jet source described in section 4. This is supported by a CE of 1% reported in [59] from what also seems to be a xenon filament or droplet target.

Tin, on the other hand, appears to be an optimal substance due to its emission peak at $\lambda = 13.5$ nm. A CE of 2.5%/(2%BW 2π sr) at $\lambda = 13.45$ nm has been obtained for a liquid-tin-jet laser plasma [44]. This is even better than the 2% assumed in the design example. However, as will be discussed in section 8, tin is a condensing material, which produces severe contamination problems that may limit its applicability. Which target material will finally turn out to be the best will depend both on the target emission characteristics and the effectiveness of different debris mitigation schemes.

7. Available collection angle and source size

As can be seen from equation (3), the available collection angle also has an impact on the power delivered to the IF. As is illustrated in figure 7, though, the liquid-jet sources have a distinct advantage in that no source hardware will geometrically obstruct the line of sight from the plasma. In this way, collectors with collection solid angles approaching $\Omega = 2\pi$ sr may theoretically be achieved. One can even envision increasing the collection angle to $\Omega > 2\pi$ sr as is illustrated by the dashed line in figure 7. Unfortunately, the collector throughput does not scale linearly with the collection solid angle since the reflectivity of a Mo/Si mirror varies with incidence angle. For example, for angles approaching 45° the reflectivity decreases significantly since the reflectivity for p-polarized EUV radiation drops to zero at 45° [60].

The available collection solid angle is, however, not only limited by the geometrical access to the plasma. The étendue of the EUVL system will limit either the collectable solid angle, Ω, or the source-area fraction ($A_{\mathrm{col}}/A_{\mathrm{tot}}$) that is collected.

Although a detailed analysis [61] is required to determine the étendue of a three-dimensional source combined with a certain collector, the étendue is roughly given by the emitting source area, A, and the numerical aperture, NA, of the collector as [62]

$$\text{étendue} = A \times \pi \times \mathrm{NA}^2, \tag{4}$$

where the relationship between NA and solid angle, Ω, is

$$\mathrm{NA} = \sqrt{1 - \left(1 - \frac{\Omega}{2\pi}\right)^2}. \tag{5}$$

As is specified in the source requirement of table 1, the étendue of the source output is limited to 1–3.3 mm^2 sr. The size of the plasma can therefore not be too large, since otherwise the available collection angle will be limited.

Figure 10 illustrates typical plasma sizes for a liquid-xenon-jet laser–plasma source [40]. The images were

acquired using an EUV camera based on a spherical multilayer mirror that was developed to obtain both wavelength selectivity and high spatial resolution simultaneously. It is preferable to use such an EUV camera instead of traditional pinhole cameras since the EUV in-band image of a plasma might not correspond to a broad-band image [63] typically obtained with pinhole cameras. Moreover, it is difficult to obtain good spatial resolution using a pinhole camera, which is especially important when imaging very small plasmas.

Due to the small dimensions of a typical liquid-jet target, very small plasmas can be achieved. Figure 10 illustrates such a plasma, $\sim$20 μm FWHM, obtained with a liquid-xenon-jet laser plasma and by focusing the laser as tightly as possible on the jet. Unfortunately, the very small plasmas have a CE, typically, somewhat lower than optimal, e.g. $\sim$0.35%/(2%BW 2π sr) for the case of figure 10(*a*). By using a laser pre-pulse to expand the target and then a defocused main laser pulse, the size of the plasma can be increased [64]. A 200–270 μm FWHM plasma is shown in figure 10(*b*). A CE of $\sim$0.95%/(2%BW 2π sr) has been shown for large plasmas. Even if the full geometrical diameter of the plasma of figure 10(*b*) is considered ($d \approx 400\,\mu$m), and a large collection angle of 2π sr (NA = 1), the resulting étendue is $\sim$0.4 mm^2, which is well below the presently estimated maximum allowable source output étendue [49]. Thus, no power from the laser–plasma source will be lost due to the étendue limitation. This is in contrast to the larger-diameter discharge sources where such loss may become important [61]. The plasma size presented above corresponds well with other liquid-jet laser–plasma studies.

8. Mirror lifetime

As briefly discussed in section 5, the collector-mirror lifetime is of great importance especially for the CoO of a source. Achieving a long mirror lifetime is, however, a delicate problem since the plasma faces the collector mirror directly with no intermediate protection. Two major mechanisms are responsible for the mirror degradation. Either the mirror surface is damaged by larger debris particles or high-energy ions and neutrals from the plasma, or the mirror is coated by some contaminant that absorbs the EUV.

8.1. Mirror surface sputtering

A laser plasma emits ions and neutrals of very high energies. The ion energies from a liquid-xenon-jet laser plasma has, e.g. been reported in [40]. The energies were measured through a time-of-flight experiment with a Faraday cup as ion detector (cf [65]). The resulting maximum ion energies as a function of laser-pulse energy and direction of measurement are illustrated in figure 11. The sputter yield at these energies, in the multi-kiloelectronvolt range, has furthermore been shown to be about unity [40]. The presence of multi-kiloelectronvolt xenon ions from plasmas created by several-nanosecond laser pulses has also been reported in other studies of similar targets [66, 81] and in solid-bulk targets [65]. Multi-kiloelectronvolt ions were, however, not found in a xenon-gas-puff target experiment [65].

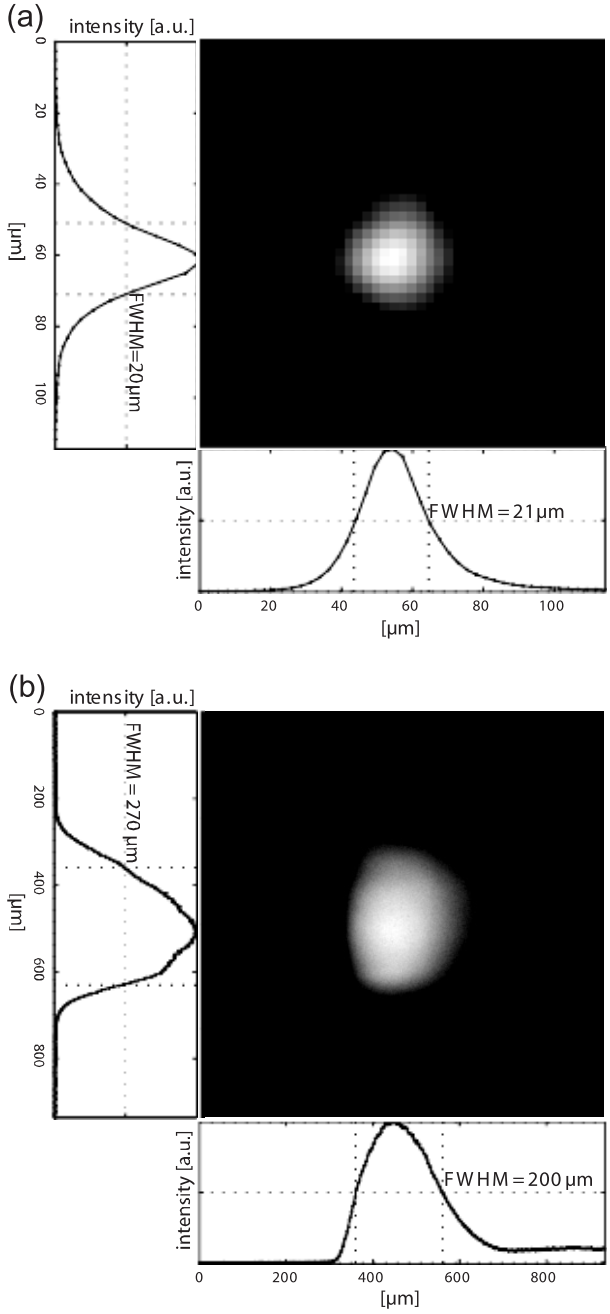

Figure 10. Images of a small plasma (five shots averaged) in (*a*) and a larger plasma (40 shots averaged) in (*b*). The emission tail in image (*b*) is an artefact due to the fact that the CCD was read out during continuous exposure (from [38]).

The existence of high-energy ions suggests that sputtering of the collector mirror and other components will be a major problem. The sputtering has also been verified by exposing witness plates (silicon wafers) to a liquid-xenon-jet laser plasma. In [40] it is reported how silicon wafers were exposed to 10^6 plasma events generated by $\sim$330 mJ laser pulses, where the wafers were placed 110 mm from the plasma. The wafers were masked except for a small area, and the edges between the masked and unmasked area were investigated with a surface profiler after the exposure. The unmasked area showed up to $\sim$27 nm deep sputtering (see figure 12).

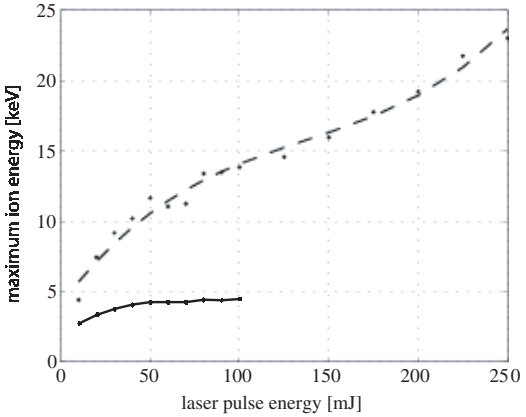

Figure 11. The dependence of laser pulse energy on maximum ion energy. The dashed line was obtained with the Faraday cup at an angle of 45° to the incoming laser beam and the solid line at 135° (from [38]).

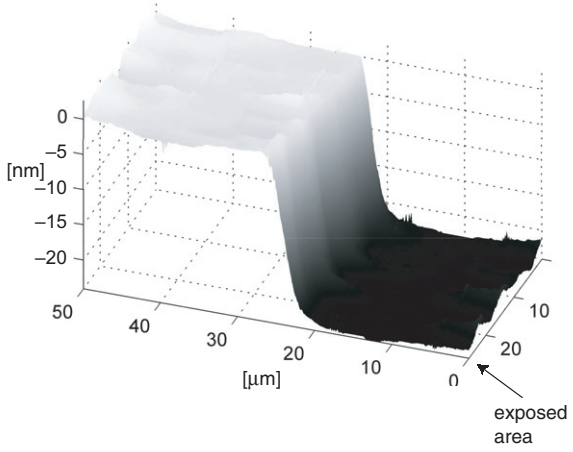

Figure 12. The edge between masked and unmasked areas of a silicon wafer exposed to 10^6 plasma events (from [38]).

The sputtering ions and neutrals have to be decelerated to non-sputtering energies before reaching the collector mirror or other components in order to meet the lifetime specification. It has been reported that a background pressure can reduce the energy of the fast ions [67, 68]. Hansson *et al* [40] reported the result of a simple experiment, where the turbo-molecular pumps of the source chamber were stopped, thereby increasing the xenon pressure in the vacuum chamber to >1 mbar. Silicon wafers were exposed under identical conditions to the previously discussed sputter experiments. Indeed, no sputtering was observed, but rather a deposition of ∼4 nm. The composition of the deposition was, however, not analysed. Although the background pressure of >1 mbar is too high since it will absorb most of the in-band EUV radiation over a short distance, at least the concept was shown. Further experiments should be performed where the background pressure can be accurately controlled, and using gases other than the highly EUV-absorbing xenon. It is important to limit the impact on the parameter T_{gas} of equation (3). Other ion-mitigation methods such as electrostatic repeller fields [69] or magnetic-field shields [70] should also be investigated. However, the introduction of such concepts without limiting the collection angle may be difficult.

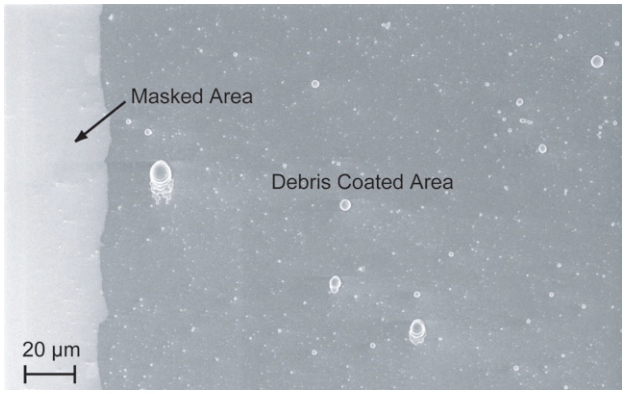

Figure 13. SEM image of debris plate 3, where the particulate debris is clearly visible on the background due to ionic/atomic debris (from [42]).

Apart from direct sputtering of the mirror surface, other source components that are in the line of sight of the plasma can be sputtered. This can lead to the release of foreign material in the source chamber that can eventually coat the surface of the mirror. If the target-delivery nozzle is in the vicinity of the plasma, sputtering of the nozzle material can be especially harmful [7]. The large working distance, though, that is achievable with liquid-jet sources may limit such nozzle sputtering. Other coating issues are discussed below.

8.2. Mirror surface coating

The biggest coating problem arises when the target material is a condensing material, such as a metal. This is well illustrated by the experiment with a liquid-tin-jet [44] where debris measurements were performed using partly masked silicon wafer substrates as witness plates at four different positions 190 mm from the plasma (cf figure 6). The witness plates were exposed for ∼15 min at 20 Hz operation and analysed by scanning electron microscopy (SEM) and surface profilometry.

Examination of the four debris plates shows that the debris emission is not distributed uniformly. The plates on the incoming laser side are sparsely covered with micrometre-sized particles (a few as large as 10–50 μm) on top of a thin background coating of 5.3 ± 1 nm (1σ) thickness. A SEM image of plate 3 is shown in figure 13, where both the darker background coating and the particles can be observed. The plate behind the incoming laser side is almost fully covered with the larger particles resulting in an average thickness of ∼700 nm where the thicker coating is probably due to non-ionic debris.

If the ionic and atomic fractions of the ejected material are assumed to correspond to a 50 μm section of the jet and are distributed in a 4π sr solid angle, the theoretical layer thickness should be of the order of ∼10 nm. Although crude, these calculations show decent quantitative agreement with the experimental data in the direction of the incoming laser beam. It can be argued that by using smaller diameter jets or droplets, the amount of particulate debris can be limited, ultimately reducing the debris problem to only the ions and atoms. However, this fraction alone produces $\sim 9 \times 10^{-7}$ g per pulse. In a future production-scale EUV lithography system operating at >7 kHz and with a 25% duty cycle [71],

this will result in an annual emission of ∼50 kg of ionic and atomic Sn, which will coat the collector mirrors positioned approximately 10 cm from the source. In order to keep the reflectivity losses of in-band EUV to <10% (i.e. <0.8 nm Sn coating) a debris mitigation efficiency of $\sim 10^8$ is therefore necessary. This will require a significant development effort since no such highly effective mitigation technique is available at present.

Apart from direct physical deposition as described above, some chemical issues are also present due to the interaction of residual gases in the chamber. The EUV radiation creates secondary electrons, which dissociate adsorbed molecules, especially hydrocarbons and water, that may be present at the mirror surface [72]. These species then react with the topmost layer, building oxide (SiO_x) and carbide (SiC) layers [73]. Such contamination layers drastically reduce the reflectivity of the mirrors. A 10% reflectivity loss is observed after growth of just 1–3 nm SiC or 0.5–1 nm SiO_x [74]. There are, however, methods to prevent this contamination, which include maintaining an ultra-clean environment with, for example, the use of UHV techniques or the use of a capping layer on the mirror to reduce the reactivity [75, 76] of its surface. To some extent, *in situ* cleaning of the mirror [77, 78] can be employed to remove the contamination, but only the carbide layers can be removed.

9. Further source characteristics

Although in-band EUV power to the IF and the source cleanliness may be the two most critical requirements to meet, several other parameters specified in table 1 have to be fulfilled. Several studies have reported on these parameters.

Different studies on the maximum repetition rate of liquid-xenon-jet sources have reached results ranging from 10–30 kHz [37, 40, 42, 79], i.e. fulfilling the requirement of table 1. It is believed that the limiting factor for the repetition rate of a liquid-xenon-jet laser–plasma source is the time after one plasma event until new unaffected target material is available at the laser-focus point. Furthermore, a liquid-water-jet laser plasma has shown [51] stable operation at 250 kHz indicating that targets in the liquid rather than the solid state may be able to sustain higher repetition rates.

As is discussed in section 5, drive-laser power of >10 kW may be needed to fulfil the power requirements of a high-volume EUV stepper. However, it is difficult to verify that the target systems can handle such powers since suitable >10 kW lasers are still not available for experiments. Instead, the thermal load on the nozzle may be simulated experimentally. An attempt to simulate high-power operation of a liquid-xenon-jet laser plasma was reported in [80]. Here, it is shown how a liquid-xenon-jet can be stably operated with a 50 W laser plasma generated 1.5 mm from the nozzle. This power load on the nozzle would compare to 40 kW at 50 mm from the nozzle. Furthermore, [80] reports on calculations that the operation of such high laser powers at >50 mm from the nozzle should only increase the xenon temperature by a few degrees, supporting the high-power simulation.

The non-EUV radiation from the plasma also has to be characterized, since this out-of-band radiation will have a negative impact on EUVL system performance. The DUV radiation, $\lambda \sim$ 130–300 nm, is especially harmful since it can expose the resist if it reaches the wafer. Longer wavelengths are also harmful, though, since they will increase the thermal load on components throughout the system. Hansson *et al* [40] report on an estimation of the DUV out-of-band radiation, concluding that the measured fraction of in-band-EUV CE to DUV CE of 39% is 5.6 times higher than the required 7%, according to the specifications in table 1. However, they also discuss how several improvements could limit this value to within the specifications. This is supported by another xenon laser–plasma experiment showing a DUV/EUV ratio at the secondary focus of 4% [81]. Meeting the out-of-band requirement is important since otherwise a spectral-purity filter will have to be applied as illustrated in figure 7, and this will absorb a significant part of the EUV in-band radiation, yielding a value of T_{SPF} (cf equation (3)) different from 100%.

10. Conclusions

We conclude that liquid-jet target laser–plasma sources are a viable alternative for the high-power EUV source necessary for high-volume EUVL. They have the suitable generic properties to allow high-power, high-repetition rate, and long-term operation in combination with low debris production. Still, significant research and development efforts are needed before the sources become sufficiently refined to operate in production-scale EUV lithography tools. The major technical areas of concern are high-energy ionic debris and long-term stable operation at high powers.

Acknowledgments

The authors gratefully acknowledge the significant contributions to the technology described in this paper from present and former colleagues at both Innolite AB and the Royal Institute of Technology, Stockholm: Magnus Berglund, Hee-June Choi, Jaco de Groot, Oscar Hemberg, Anders Holmberg, Emmanuelle Janin, Björn Jacobsson, Per A C Jansson, Sofia Mosesson, Michael Otendal, Lars Rymell, Jalmar Thoresen and Martin Wilner.

References

[1] *Proc. 1st EUVL Symp. (Dallas, 2002)* CD-ROM www.sematech.org
Proc. 2nd EUVL Symp. (Antwerpen, 2003) CD-ROM www.sematech.org
[2] Attwood D 1999 *Soft X-Rays and Extreme Ultraviolet Radiation* (New York: Cambridge University Press)
[3] Franken H, Watanabe Y and Ota K 2003 Joint spec ASML, Canon, Nikon, presented at *EUVL Source Workshop (Antwerpen, Belgium)* www.sematech.org
[4] Turco I C E and Dance J B 1999 *X-Rays from Laser Plasmas* (Chichester: Wiley)
[5] Bobkowski R and Fedosejevs R 1996 Particle emission debris from a KrF laser–plasma x-ray source *J. Vac. Sci. Technol.* B **14** 1973–80
[6] Fiedorowicz H, Bartnik A, Patron Z and Parys P 1993 X-ray emission from laser-irradiated gas puff targets *Appl. Phys. Lett.* **62** 2778–80
[7] Kubiak G D, Bernardez L J and Krenz K 1998 High-power extreme ultraviolet source based on gas jets *Proc. SPIE* **3331** 81–9

[8] Fiedorowicz H, Bartnik A, Patron Z and Parys P 1994 Generation of nanosecond soft x-ray pulses as a result of interaction of the Nd : glass laser radiation with gas puff targets *Laser Part. Beams* **12** 471–83
[9] McPherson A, Luk T S, Thompson B D, Borisov A B, Shiryaev O B, Chen X, Boyer K and Rhodes C K 1994 Multiphoton induced x-ray emission from Kr clusters on M-shell (∼100 Å) and L-shell (∼6 Å) transitions *Phys. Rev. Lett.* **72** 1810–13
[10] Kubiak G D, Bernardez L J, Krenz K D, O'Connell D J, Gutowski R and Todd A M M 1996 Debris-free EUVL sources based on gas jets *OSA Trends Opt. Photonics* **4** 66–71
[11] Moyer R H, Shields H, Martos A, Fornaca S W, St Pierre R J and Petach M B 2001 Laser-produced plasma (LPP) scale-up and commercialization *Proc. SPIE* **4343** 249–54
[12] Segers M, Bougeard M, Caprin E, Ceccotti T, Normand D, Schmidt M and Sublemontier O 2002 Development of a laser-produced plasma source at 13.5 nm for the French extreme ultraviolet lithography test bench *Microelectron. Eng.* **61–62** 139–44
[13] Rymell L and Hertz H M 1993 Droplet target for low-debris laser–plasma soft x-ray generation *Opt. Commun.* **103** 105–10
[14] Malmqvist L, Rymell L, Berglund M and Hertz H M 1996 Liquid-jet target for laser–plasma soft x-ray generation *Rev. Sci. Instrum.* **67** 4150–3
[15] Lin S P and Reitz R D 1998 Drop and spray formation from a liquid jet *Annu. Rev. Fluid Mech.* **30** 85
[16] Otendal M, Hemberg O and Hertz H M 2004 Microscopic high-speed liquid–metal jets in vacuum *Experiments in Fluids* submitted
[17] Rayleigh L 1879 On the instability of jets *Proc. Lond. Math. Soc.* **10** 4–13
[18] Weber C 1931 Zum Zerfall eines Flüssigkeitsstrahles *Z. Angew. Math. Mech.* **11** 136–9
[19] Lefebvre A H 1989 Atomization and sprays *Combustion: An International Series* (New York: Hemisphere)
[20] Hansson B A M, Berglund M, Hemberg O and Hertz H M 2004 Stabilization of liquified-inert-gas jets for laser–plasma generation *J. Appl. Phys.* **95** 4432–7
[21] Rymell L, Berglund M and Hertz H M 1995 Debris-free single-line laser–plasma x-ray source for microscopy *Appl. Phys. Lett.* **66** 2625–7
[22] Hertz H M, Rymell L, Berglund M and Malmqvist L 1995 Debris-free soft x-ray generation using a liquid droplet laser–plasma target *Proc. SPIE* **2523** 88–93
[23] Richardsson M, Torres D, DePriest C, Jin F and Shimkaveg G 1998 Mass-limited, debris-free laser–plasma EUV source *Opt. Commun.* **145** 109
[24] Richardson M, Gäbel K, Jin F and Silfvast W T 1993 *OSA Proc. on Soft X-Ray Projection Lithography* vol 18 pp 156–62
[25] Rymell L and Hertz H M 1995 Debris-elimination in a droplet-target laser–plasma soft x-ray source *Rev. Sci. Instrum.* **66** 4916
[26] Tanimoto M 1972 *Proc. 7th Symp. on Fusion Technology (Grenoble)* pp 267–72
[27] Schwenn U and Sigel R 1974 *J. Phys.* E **7** 715–18
[28] Foster C A, Hendricks C D and Turnbull R J 1975 *Appl. Phys. Lett.* **26** 580–1
[29] Hertz H M, Malmqvist L, Rymell L and Berglund M 1999 Method and apparatus for generating x-ray or EUV radiation *US Patent* No 6,002,744
[30] Berglund M, Rymell L, Wilhein T and Hertz H M 1998 Cryogenic liquid-jet target for debris-free laser–plasma soft x-ray generation *Rev. Sci. Instrum.* **69** 2361
[31] Rymell L, Berglund M, Hansson B A M and Hertz H M 1999 X-ray and EUV laser–plasma sources based on cryogenic liquid-jet target *Proc. SPIE* **3676** 421
[32] Hansson B A M, Rymell L, Berglund M and Hertz H M 2000 A liquid xenon-jet laser–plasma x-ray and EUV source *Microelectron. Eng.* **53** 667
[33] Wieland M, Wilhein T, Faubel M, Ellert Ch, Schmidt M and Sublemontier O 2001 EUV and fast ion emission from cryogenic liquid-jet target laser-generated plasma *Appl. Phys.* B **72** 591
[34] Hemberg O, Hansson B A M and Hertz H M 2000 Target analysis of laser–plasma droplet-target system *Proc. SPIE* **4144** 38–42
[35] Foster C A, Kim K, Turnbull R J and Hendricks C D 1977 *Rev. Sci. Instrum.* **48** 625–31
[36] Trostell B 1995 *Nucl. Instrum. Methods Phys. Res.* A **362** 41–52
[37] Shields H, Fornaca S W, Petach M B, Michaelian M, McGregor R D, Moyer R H and St Pierre R J 2002 Xenon target performance characteristics for laser-produced plasma EUV sources *Proc. SPIE* **4688** 94–101
[38] Endo A 2004 EUV light source development at EUVA *EUVL Source Workshop (Santa Clara, California, 22 February 2004)* www.sematech.org
[39] Stamm U *et al* 2003 XTREME technologies EUV sources—an update, presented at *EUVL Source Workshop (Antwerpen, Belgium)* www.sematech.org
[40] Hansson B A M *et al* 2004 Characterization of a liquid-xenon-jet laser–plasma extreme ultraviolet source *Rev. Sci. Instrum.* **75** 2122–9
[41] Stuik R, Constantinescu R C, Hegeman P, Jonkers J, Fledderus H F, Banine V and Bijkerk F 2000 Portable diagnostics for EUV light sources *Soft x-ray and EUV imaging systems: Proc. SPIE* **4146** 121–7
[42] Abe T *et al* 2004 Performance of a 10 kHz laser-produced-plasma light source for EUV lithography *Proc. SPIE* **5374** 100–7
[43] Barthod B 2004 Modular laser produced plasma source for EUV lithography *EUVL Source Workshop (Santa Clara, California, 22 February 2004)* www.sematech.org
[44] Jansson P A C, Hansson B A M, Hemberg O, Otendal M, Holmberg A, de Groot J and Hertz H M 2004 Liquid-tin-jet laser–plasma extreme ultraviolet generation *Appl. Phys. Lett.* **84** 2256–8
[45] Hemberg O, Otendal M and Hertz H M 2003 *Appl. Phys. Lett.* **83** 1483
[46] Koay C-S, Keyser C K, Takenoshita K, Fujiwara E, Al-Rabban M M, Richardson M C, Turcu I C E, Rieger H, Stone A and Morris J H 2003 High-conversion-efficiency tin material laser–plasma source for EUVL *Proc. SPIE* **5037** 801–6
[47] Richardson M EUV, XUV and x-ray wavelength sources created from laser plasma produced from liquid metal solutions *US Patent Application* US2002070353
[48] Tompkins R J *et al* 1998 5–20 keV laser-induced x-ray generation at 1 kHz from a liquid-jet target *Rev. Sci. Instrum.* **69** 3113–7
[49] Franken H, Watanabe Y and Ota K 2003 Joint spec ASML, Canon, Nikon, presented at *EUVL Source Workshop (Antwerpen, Belgium)* www.sematech.org
[50] Banine V, Benschop J P, Leenders M and Moors R 2000 Relationship between an EUV source and the performance of an EUV lithographic system *Proc. SPIE* **3997** 126–35
[51] Vogt U, Stiel H, Will I, Wieland M, Wilhein T, Nickles P V and Sandner W 2001 Scaling-up a liquid water jet laser plasma source to high average power for extreme ultraviolet lithography *Proc. SPIE* **4343** 535–42
[52] Constantinescu R C, Jonkers J, Hegeman P and Visser M 2000 Laser-generated water plasma source for extreme-ultraviolet lithography and at-wavelength interferometry *Proc. SPIE* **4146** 101–12
[53] Vogt U, Stiel H, Will I, Nickles P V, Sandner W, Wieland M and Wilhei T 2001 Influence of laser intensity and pulse

duration on the extreme ultraviolet yield from a water jet target plasma *Appl. Phys. Lett.* **79** 2336
[54] Hansson B A M, Rymell L, Berglund M, Hemberg O, Janin E, Thoresen J and Hertz H M 2001 Liquid-xenon-jet laser–plasma source for EUV lithography *Proc. SPIE* **4506** 1–8
[55] Carroll P K and O'Sullivan G 1982 Ground-state configurations of ionic species I through XVI for $Z = 57$–74 and the interpretation of 4d-4f emission resonances in laser-produced plasmas *Phys. Rev.* A **25** 275–86
[56] Mandelbaum P, Finkenthal M, Schwob J and Klapisch M 1987 Interpretation of the quasicontinuum band emitted by highly ionized rare-earth elements in the 70–100 Å range *Phys. Rev.* A **35** 5051–9
[57] Zeng G M, Daido H, Nishikawa T, Takabe H, Nakayama S, Aritome H, Murai K, Kato Y, Nakatsuka M and Nakai S 1994 Soft x-ray spectra of highly ionized elements with atomic numbers ranging from 57 to 82 produced by compact lasers *J. Appl. Phys.* **75** 1923–30
[58] Svendsen W and O'Sullivan G 1994 Statistics and characteristics of xuv transition arrays from laser-produced plasmas of the elements tin through iodine *Phys. Rev.* A **50** 3710–18
[59] Stamm U *et al* 2004 *Proc. SPIE* **5374** 1331–44
[60] Center for X-Ray Optics (CXRO) Program for calculation of multilayer-mirror reflectivity www-cxro.lbl.gov/optical_constants/multi2.html
[61] Derra G H and Singer W 2003 Collection efficiency of EUV sources *Proc. SPIE* **5037** 728–41
[62] Antoni M, Singer W, Schultz J, Wangler J, Escudero-Sanz I and Kruizinga B 2000 Illumination optics design for EUV lithography *Proc. SPIE* **4146** 25–34
[63] Fomenkov I V, Ness R M, Oliver I R, Melnychuk S T, Khodykin O V, Bowering N R, Rettig C L and Hoffman R 2003 Performance and scaling of a dense plasma focus light source for EUV lithography *Proc. SPIE* **2003** 807–21
[64] Hansson B A M, Berglund M, Hemberg O and Hertz H M 2000 Xenon liquid-jet laser–plasma source for EUV lithography, presented at *2nd Annual Int. Workshop on EUV Lithography (San Francisco, California)* www.sematech.org
[65] Daido H, Yamagami S, Suzuki M, Azuma H, Choi I W and Fiedorowicz H 2001 Low-energy ion emission from a xenon gas-puff laser–plasma x-ray source *Appl. Phys.* B **71** 385–7
[66] Endo A 2003 EUV light source development at EUVA, presented at *EUVL Source Workshop (Antwerpen, Belgium)* www.sematech.org
[67] Ginter M L and McIlrath T J 1988 Debris and VUV emission from a laser-produced plasma operated at 150 Hz using a krypton fluoride laser *Appl. Opt.* **27** 885–9
[68] Shmaenok L *et al* 1994 Issues of laser plasma sources for soft x-ray projection lithography *Microelectron. Eng.* **23** 211–14
[69] Takenoshita K, Koay C-S, Richardson M C and Turcu I C E 2003 Repeller field debris mitigation approach for EUV sources *Proc. SPIE* **5037** 792–800
[70] Niimi G, Ueno Y, Nishigori K, Aota T, Yashiro H and Tomie T 2003 Repeller field debris mitigation approach for EUV sources *Proc. SPIE* **5037** 370–7
[71] Franken H, Watanabe Y and Ota K 2003 Joint Spec ASML, Canon, Nikon, presented at *EUVL Source Workshop (Antwerp)* www.sematech.org
[72] Boller K, Haelbich R-P, Hogrefe H, Jark W and Kunz C 1983 Investigation of carbon contamination of mirror surfaces exposed to synchrotron radiation *Nucl. Instrum. Methods Phys. Res.* **208** 273–9
[73] Wedowski M, Bajt S, Folta J, Gullikson E, Kleineberg U, Klebanoff L, Malinowski M and Clift W 1999 Lifetime studies of Mo/Si and Mo/Be multilayer coatings for extreme ultraviolet lithography *Proc. SPIE* **3767** 217–24
[74] Mertens B *et al* 2001 Mitigation of molecular contamination of EUV optics, presented at *3rd Int. Workshop on EUV Lithography (Matsue, Japan)* www.sematech.org
[75] Malinowski M, Steinhaus C, Clift M, Klebanoff L, Mrowska S and Soufli R 2002 Controlling contamination in Mo/Si multilayer mirrors by Si surface-capping modifications *Proc. SPIE* **4688** 442–53
[76] Klebanoff L, Clift W, Malinowski M, Steinhaus C, Grunow P and Bajt S 2002 Radiation-induced protective carbon coating for extreme ultraviolet optics *J. Vac. Sci. Technol.* B **20** 696–703
[77] Klebanoff L E 2000 First environmental data from the engineering test stand (ETS), presented at *2nd Annual Int. Workshop on EUV Lithography* www.sematech.org
[78] Malinowski M, Klebanoff L, Grunow P, Steinhaus C and Clift M 2000 Use of molecular oxygen to reduce EUV-induced carbon contamination of optics, presented at *2nd Annual Int. Workshop on EUV Lithography* www.sematech.org
[79] Hansson B A M, Lars R, Berglund M, Hemberg O E, Janin E, Thoresen J, Mosesson S, Wallin J and Hertz H M 2002 Status of the liquid-xenon-jet laser–plasma source for EUV lithography *Proc. SPIE* **4688** 102–9
[80] Hansson B A M 2002 Status of the liquid-xenon-jet laser–plasma source, presented at *EUV Source Workshop (Dallas, Texas)* www.sematech.org
[81] 2002 TRW/cutting edge optronics laser-produced plasma EUV source program, presented at *EUV Source Workshop (Dallas, Texas, 2002)* www.sematech.org